JOURNAL OF GEOPHYSICAL RESEARCH, VOL. 103, NO. D1, PAGES 1573–1583, JANUARY 20, 1998

Aerosol size distributions obtained from HALOE spectral extinction measurements

Mark E. Hervig and Terry Deshler

Department of Atmospheric Science, University of Wyoming, Laramie

James M. Russell III

Center for Atmospheric Sciences, Hampton University, Hampton, Virginia

Abstract. A technique was developed to use multiwavelength aerosol extinction measurements from the Halogen Occultation Experiment (HALOE) to determine the size distribution of stratospheric H_2O–H_2SO_4 aerosols. Although the HALOE extinction spectrum alone cannot be used to reliably infer the aerosol size distribution (except when the aerosol population contains particles larger than about 0.5 μm), the inverse problem becomes highly defined when the effective radius is known. Using theoretical relationships derived from in situ aerosol measurements, we found that the effective radius can be determined from the HALOE 2.45 μm extinction with uncertainties of about ±15%. Using extinction ratios with the effective radii determined from the HALOE extinctions, we obtained unimodal lognormal size distributions. The HALOE size distributions are generally unbiased with respect to coincident in situ aerosol measurements. Error analysis reveals that uncertainties in the inferred surface areas and volumes are less than 30% and 15%, respectively. Inferring size distributions from the HALOE data set provides global and temporal aerosol information, which can satisfy important needs for investigations of the Earth's radiative and chemical balance.

1. Introduction

An extensive global record of remote aerosol measurements has been obtained since the advent of satellite–borne sensors in the 1970s. The most directly measured quantity, optical cross section per unit volume, is useful for characterizing the aerosol spatial and temporal distribution but is of limited use in chemical and radiative transfer studies, which require the aerosol size distribution and/or the distribution moments (for example, surface area). Early in this century, *Angstrom* [1908] realized that the particle size is related to the wavelength dependence of extinction. By taking advantage of this relationship, multiwavelength aerosol extinction measurements can be used to infer aerosol size distributions [e.g., *Yue et al.*, 1986]. Because of the usefulness of aerosol size distributions, significant effort has been applied to this inversion problem [e.g., *Curcio*, 1961; *King et al.*, 1978; *Valero and Pilewskie*, 1992]. Here we contribute to this effort through the development of an inversion method using multiwavelength aerosol extinction measurements from the Halogen Occultation experiment (HALOE). The method described here is valid only for H_2O–H_2SO_4 (sulfate) aerosols.

HALOE is on board the Upper Atmosphere Research Satellite and began science observations on October 11, 1991. The HALOE instrument uses the principle of satellite solar occultation and the instrumental techniques of gas filter radiometry and broadband radiometry to measure profiles of solar attenuation by the atmosphere's limb, as the Sun rises or sets in relation to the spacecraft. Measurements in eight spectral bands (from 2.45 to 10.01 μm) are used to retrieve the profiles of HF, HCl, CH_4, NO, NO_2, H_2O, and O_3 mixing ratios, temperature, and aerosol extinction at 2.45, 2.80, 3.40, 3.46, and 5.26 μm wavelengths. HALOE measurements cover two longitude sweeps each day (15 profiles each), one at the latitude of sunsets and one at the latitude of sunrises. Adjacent HALOE sunrise (or sunset) measurements are separated by 1.6 hours and 24° longitude (which is 1900 km at 45° latitude). The progression of measurement latitude with time provides near–global coverage over periods of 3–4 weeks. A complete description of the experiment is given by *Russell et al.* [1993]. The HALOE aerosol retrievals are described in detail by *Hervig et al.* [1995], and a validation of these measurements is presented by *Hervig et al.* [1996].

HALOE observations are accurately registered in altitude, and the vertical resolution of the aerosol measurements is ~2 km. The sample volume length (along the limb) is determined mainly by the vertical resolution, and this dimension is roughly 320 km. The sample volume width (across the limb) is determined mainly by the angle between the orbit plane and the satellite–Sun vector and ranges from 6 to 50 km. Since the HALOE signals are spatially averaged, variability on sub–sample volume scales will be suppressed. This effect is a concern for measurements of localized episodes, such as stratospheric or tropospheric clouds, and for measurements in the presence of strong gradients, as are produced after volcanic injections. While spatial averaging is less of a concern under quiescent conditions, the net effect has not been quantitatively assessed. This fact should be borne in mind in comparing HALOE with measurements with finer spatial resolution, as we have done later in this paper.

This work begins by establishing theoretical relationships between the physical and optical properties of sulfate aerosols and simulated extinctions at the HALOE wavelengths. These simulations are then used to investigate the information content of the multi–wavelength extinctions. The inversion procedure is described, and error analyses are presented. Finally, results obtained from the HALOE measurements are compared with coincident in situ observations.

Paper number 97JD03081.
0148–0227/98/97JD–03081$09.00

For the inversions presented below, the extinctions at only three HALOE wavelengths were used (2.45, 3.40, and 5.26 μm). The HALOE aerosol measurements at 3.40 and 3.46 μm are redundant, as only ±5% variations in extinction are predicted for a wide range of aerosol sizes and refractive indices. The 2.80 μm aerosol extinction measurements were eliminated on the basis of the large uncertainties, lack of internal consistency, and poor agreement with independent measurements [*Hervig et al.*, 1996].

2. Physical and Optical Properties of Stratospheric Sulfate Aerosols

2.1 Composition

For temperatures warmer than about 200 K, stratospheric aerosol are a binary mixture of H_2SO_4 and H_2O [*Rosen*, 1971]. The equilibrium composition of sulfate aerosols (weight percent of H_2SO_4 in the mixture, W_s) may be determined as a function of temperature and partial pressure of water vapor [*Steele and Hamill*, 1981]. Steele and Hamill have calculated the equilibrium composition of sulfate aerosol for temperatures (T) from 190 to 260 K and water vapor pressures (p_w) from 2 to 30 $\times 10^{-4}$ mbar. *Hanson et al.* [1994] report a fit to the Steele and Hamill data for W_s in terms of T and p_w, which was used to determine W_s throughout this work.

2.2 Size distribution

Understanding of the relationship between aerosol size and concentration has been gained by using a variety of measurement techniques. A large body of aerosol measurements has shown that the size distribution can be adequately described by using a functional form (for example, power law, modified gamma, exponential, lognormal, and zold [e.g., *Junge*, 1952; *King et al.*, 1978]). The impaction/collection measurements reported by *Goodman et al.* [1994] and *Pueschel et al.* [1994] and the optical particle counter (OPC) measurements reported by *Pinnick et al.* [1976] and *Deshler et al.* [1993] were best described by using the lognormal distribution,

$$n(r)dr = \sum_{i=1}^{k} N_i \frac{\exp\left[\ln^2 (r/\bar{r}_i) / (2 \ln^2 \sigma_i)\right]}{r\,(2\pi)^{(1/2)}\,\ln(\sigma_i)} \qquad (1)$$

where $n(r)$ is the differential concentration in the radius interval dr, k is the number of modes in the distribution, N_i is the number concentration, σ_i is the distribution width, and $\bar{r}_i$ is the median radius, for each of i modes.

Routine profile measurements of aerosols using OPCs have been conducted over Laramie, Wyoming (41°N) since the early 1970s [e.g., *Hofmann and Rosen*, 1983], comprising the most extensive record of in situ size distribution profile measurements available. Since these measurements are described with the use of lognormal size distributions and since there are physical reasons to expect a lognormal form for an aerosol distribution [*Granqvist and Buhrman*, 1976], this work will focus on the lognormal form. Although the OPC measurements are usually best described with the use of a bimodal distribution, especially in postvolcanic periods [*Deshler et al.*, 1993], a single-mode distribution can be fitted to the data. Lognormal fits that poorly characterized the original OPC measurements were discarded for this work (about 25% of the unimodal fits and 15% of the bimodal fits). Laramie aerosol measurements covering June 1991 to June 1997 at altitudes above the tropopause are used to understand the physical range of sulfate aerosol size distributions during the Pinatubo volcanic cycle.

Figure 1a shows the median radii and distribution width for unimodal lognormal fits to the Laramie OPC data, where typical

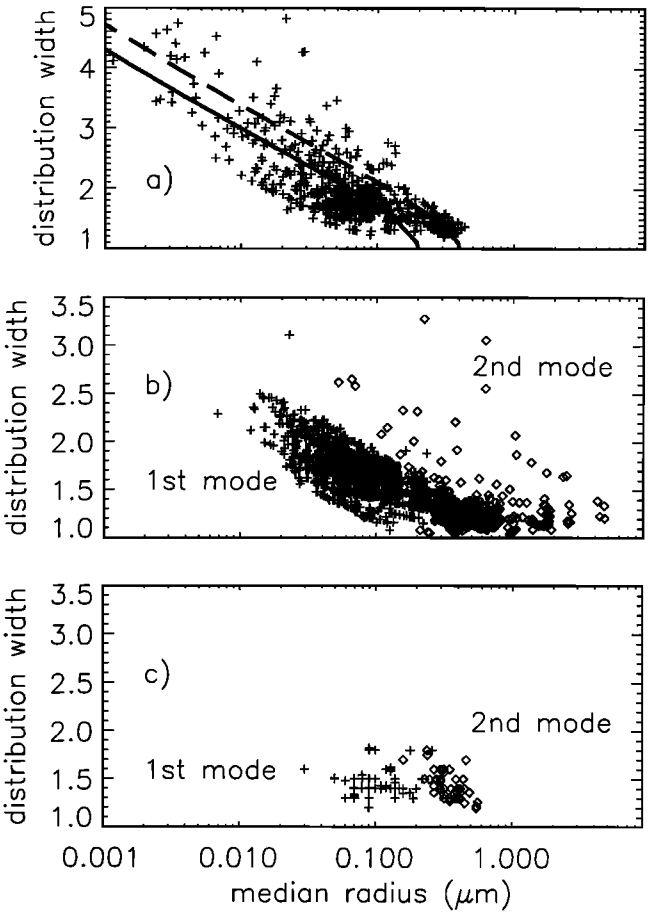

Figure 1. (a) Unimodal fits to the Laramie OPC data (551 distributions). The lines show the relationship between σ and $\bar{r}$ from equation (2) for constant values of the effective radius: 0.2 μm (solid) and 0.4 μm (dashed). (b) First and second modes of bimodal fits to the Laramie OPC data (872 distributions). Laramie data in Figures 1a and 1b are from 63 profiles measured in sulfate aerosols during June 1991 to June 1997, and data for all altitudes above the tropopause are shown. (c) First and second modes of bimodal lognormal fits to impactor/collector data measured in sulfate aerosols, as reported by *Goodman et al.* [1994] (21 distributions, Table 1 in reference) and by *Pueschel et al.* [1994] (35 distributions, Table 1a in reference). The data were collected during February 1991 to May 1993 at altitudes typically from 18 to 20 km and latitudes between about 20°N and 70°N.

distributions have median radii from 0.01 to 0.3 μm and widths from 1 to 3. It is apparent from Figure 1 that the distribution width and median radius are dependent on each other. The general trend for narrower distributions to be characterized by larger particles is consistent with condensational growth theory. Since the growth rate of a solution drop (dr/dt) increases with decreasing radius, smaller particles grow faster [*Pruppacher and Klett*, 1980], narrowing the distribution. The relationship between σ and $\bar{r}$ can also be understood by computing σ versus $\bar{r}$ for constant values of the aerosol effective radius, or area-weighted mean radius ($R_e = 3V/S$, where V is volume and S is surface area). Measurements indicate that R_e is a slowly varying quantity in the stratosphere [e.g., *Russell et al.*, 1996] (Figure 10). A relationship between σ and $\bar{r}$ was derived for unimodal lognormal size distributions by using (1) to calculate S and V and thus R_e.

$$\bar{r} = R_e \exp\left[-5\,(\ln^2\sigma)/2\right] \qquad (2)$$

Relationships between σ and $\bar{r}$ determined by using (2) are shown in

Figure 1a for constant values of R_e (0.2 and 0.4 μm). While this simple parameterization does not entirely explain the observations, it does capture the general dependence between σ and $\bar{r}$. Figure 1b shows the median radii and widths for both modes of the bimodal fits to the Laramie data. The first modes of the bimodal distributions occur at smaller median radii and are narrower than the unimodal distributions, since the large particles are described by the second mode.

For comparison the median radii and widths for lognormal size distributions reported by *Goodman et al.* [1994] and *Pueschel et al.* [1994] are shown in Figure 1c. These data were measured at altitudes typically from 18 to 20 km and therefore do not cover the broad range of conditions shown for the OPCs. The general dependence between σ and $\bar{r}$ from these data, however, is consistent with the Laramie OPC data.

2.3. Scattering and absorption theory

Sulfate aerosols are considered to be spheres, which is a good assumption, and thus the scattering and absorption of radiation by an individual aerosol can be described by using Mie theory. The extinction coefficient, β_e, for a population of aerosols is calculated by integrating the extinction efficiency (Q_e, defined as optical cross section/geometric cross section) over the size distribution:

$$\beta_e(\lambda) = \int_{r_1}^{r_2} \pi r^2 Q_e(r,\lambda,m)\, n(r)\, dr \qquad (3)$$

where λ is wavelength, m is refractive index, and r_1 and r_2 are the smallest and largest radii in the size distribution.

2.4. Refractive index

The complex refractive index of a sulfate aerosol is determined by the aerosol's composition, the measurement wavelength, and temperature. The measured refractive indices of sulfuric acid solutions are given by *Palmer and Williams* [1975] at 300 K for wavelengths from 0.3 to 25.0 μm and compositions from 25% to 95%. *Remsberg et al.* [1974] have reported sulfate refractive indices at 296 K for wavelengths from 6 to 13 μm and compositions of 75% and 90%. Although the imaginary indices of Remsberg et al. are greater than the Palmer and Williams values, there is no reason to suspect the shorter-wavelength data of Palmer and Williams, which are used throughout this work. Linear interpolations in wavelength and composition were used to determine complex refractive indices for the HALOE wavelengths and a complete range of stratospheric aerosol compositions. The indices were adjusted to stratospheric temperatures by using the Lorentz–Lorenz rule with the solution densities from *Luo et al.* [1997]. This procedure results in relatively small changes in the indices.

2.5. Measurement simulation

Since the number of inferred parameters is limited to the number of measurements, the extinction simulations must be formulated by using no more than three parameters. We have used the unimodal lognormal size distribution (equation (1)) in the simulations reported here, and thus the retrieved quantities are N, σ, and $\bar{r}$. The equilibrium sulfate aerosol composition is determined by using the measured water vapor mixing ratio from HALOE (uncertainties of about ±10% [*Harries et al.*, 1996]), and the corresponding temperature and pressure. The spectral refractive index versus composition data of *Palmer and Williams* [1975] were used to describe the refractive indices for all wavelengths as a function of the composition alone. Inverting measurements of particles not described by this model could produce erroneous results.

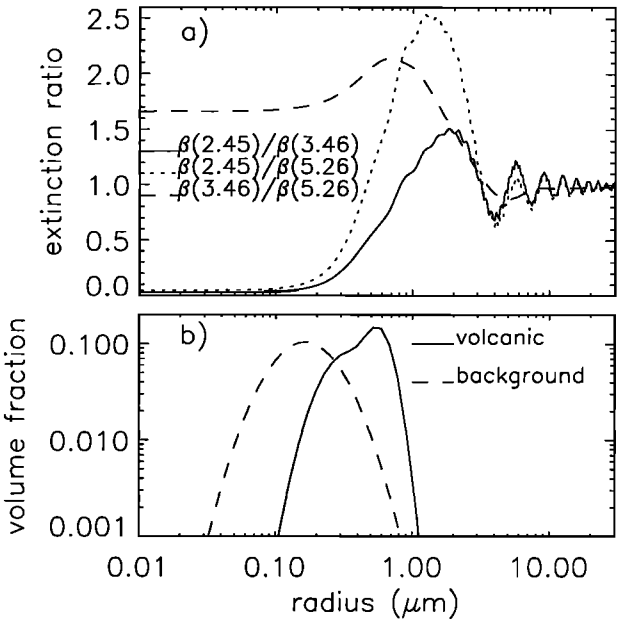

Figure 2. (a) Ratios of extinction at different wavelengths (as labeled) versus particle radius calculated for 75% H_2SO_4. (b) Aerosol volume distributions as fraction of total volume versus particle radius, representing typical background and volcanic (Pinatubo) conditions.

3. Information Content of Multiwavelength Extinction Measurements

It is important to determine the ability of the extinction measurements to detect and resolve the aerosol size, or more practically, aerosols within specific size regimes. The sizing information comes from spectral variations in extinction, or interchannel variability. This variability can be qualitatively assessed by examining the single-particle extinction ratios versus radius. The ratios $R_1=\beta_e(2.45)/\beta_e(3.46)$, $R_2=\beta_e(2.45)/\beta_e(5.26)$, and $R_3=\beta_e(3.46)/\beta_e(5.26)$ calculated for 75 wt% H_2SO_4 are shown in Figure 2 together with representative aerosol volume distributions. All three ratios are constant for radii of <0.1 μm, indicating that these sizes are inseparable from each other. For increasing radius, R_1 and R_2 increase sharply, and the presence of sizes >0.1 μm should therefore be indicated by these ratios. R_3 shows smaller variations over the typical range of sizes (see the volume distributions, Figure 2b) and therefore contains less information that would indicate the presence of different size regimes.

The total number concentration (N) can be moved outside the integral over radius in computing the total extinction for a unimodal lognormal size distribution (equations (1) and (3)). As a result the specific relationships between spectral extinction and size distribution are determined by σ and $\bar{r}$ alone (for a given composition). Integration over the size distribution adds the extinction contributions from the different size regimes. Aerosol with radii greater than about 1 μm, however, exist at very low concentrations (see Figure 2). As a result the integration occurs over an essentially monotonic function and therefore has a direct dependence on $\bar{r}$ for a given σ, or on σ for a given $\bar{r}$. The response of the extinction spectra to changes in the size distribution can therefore be qualitatively understood by inspection of Figure 2.

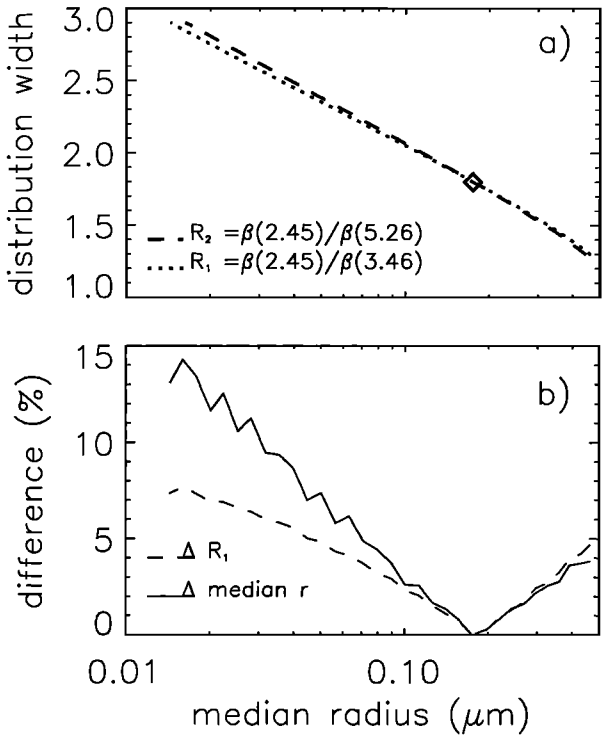

Figure 3. (a) All size distributions that give the same extinction ratios, R_1 or R_2, as were calculated by using the distribution $\sigma = 1.8$ and $\bar{r} = 0.17$ μm, for 75% H_2SO_4. Only the single assumed distribution (diamond) reproduces both extinction ratios (i.e., the solution to the inverse problem). (b) Difference between the median radii for the distribution that reproduced R_1 and R_2 (Δ median r), and the difference between the target value of R_1 and the value of R_1 computed from the distribution that describes R_2, $\Delta R_1 = R_1(r_1, \sigma_1) - R_1(r_2, \sigma_2)$. The differences are shown versus median radius, and are directly transposable to the widths in Figure 3a, via the curve for R_1 in Figure 3a.

A given combination of σ and $\bar{r}$ determines a unique set of extinction ratios, R_i; however, a given set of R_i can often be determined from a wide range of distributions. The question, then, is how many distributions (sets of σ and $\bar{r}$) will yield a particular set of extinction measurements. This question was answered by calculating the set of extinction ratios for one size distribution and then searching a wide range of σ and $\bar{r}$ for combinations that will also reproduce the set of extinction ratios. An example is shown in Figure 3, where R_1 and R_2 were calculated for the size distribution $\sigma = 1.8$ and $\bar{r} = 0.17$ μm, and the curves indicate all distributions that can reproduce R_1 and R_2. R_3 is typically reproduced by such a broad range of distributions that this ratio offers little sizing information. Also shown are the differences between median radii for the distributions that reproduced each measurement separately, along with the differences between the target value of R_1 and the R_1 calculated from the distributions that describe R_2 (i.e., the accuracies required for the forward and inverse problems, Figure 3b). If only one size distribution could reproduce the combination of measurements, then this distribution could be considered a unique solution to the inverse problem. For the case shown in Figure 3, such a solution exists; however, it is very poorly determined because a broad range of distributions can match the simulated combination of measurements for a change in median radius of less than 15% or for a change in one measurement of less than 8%. It would therefore be unrealistic to expect any real measurements to reliably fit a unique distribution within this size regime. For decreasing median radii, solutions to the inverse problem become increasingly ambiguous, since the distributions that will explain each measurement begin to converge.

A major cause of these problems is that a high degree of linear dependence exists among infrared extinctions [e.g., *Twomey*, 1974]. As a result the extinctions at different wavelengths tend to vary in a systematic fashion for changes in particle size. Although infrared extinctions at several wavelengths are limited by these effects, the size distribution moments exhibit a dependence on aerosol size distinctly different from that of extinction. The effective radius, as a ratio of two moments, offers definite advantages in this respect. Recall that for unimodal distributions R_e is dependent only on the distribution shape (σ and $\bar{r}$, equation (2)).

Infrared aerosol extinctions are strongly correlated with the size distribution moments (volume and surface area), and these correlations can be used to determine the moments with reasonable uncertainties [e.g., *Livingston and Russell*, 1989; *Grainger et al.*, 1995]. Following this lead, we have explored the relationship between effective radius and 2.45 μm extinction. From the record of size distributions measured using OPCs over Laramie, the relationship between R_e and $\beta_e(2.45)$ was computed for all altitudes above the tropopause. Detailed analysis reveals that the relationship between R_e and $\beta_e(2.45)$ has a small dependence on pressure, which is realized by an increase in the compactness of the relationship when only discrete pressure intervals are considered. For example, the relationship between R_e and $\beta_e(2.45)$ only for pressures between 30 and 40 mbar is shown in Figure 4. Based on relationships as in Figure 4 for a number of pressure intervals, the dependence of R_e on $\beta_e(2.45)$ was found to follow a power law,

$$R_e = A\,\beta_e(2.45)^B \tag{4}$$

where the pressure dependence of the empirical constants A and B were described with the use of polynomials (Figure 5). Capturing the pressure dependence of these conversions offers 5–10% uncertainty reductions in the determination of R_e over pressure independent conversions. Since $R_e = 3V/S$, and S and V have generally the same altitude dependence, R_e is not strongly dependent on altitude (see Figure 8, for example). Extinction on the other hand, can vary by 3 orders of magnitude over the range of stratospheric altitudes. It is

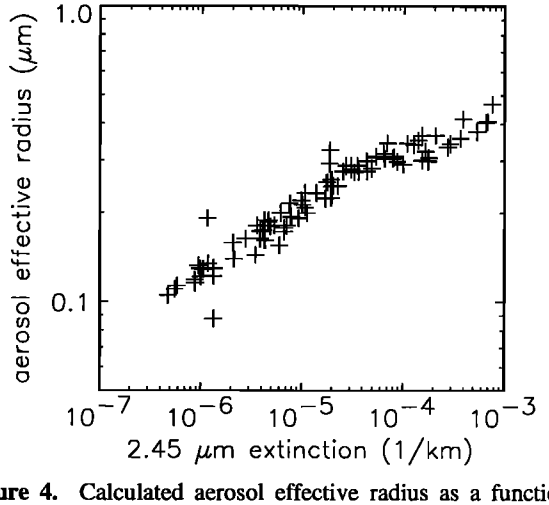

Figure 4. Calculated aerosol effective radius as a function of calculated 2.45 μm extinction using the Laramie size distributions for profiles measured from June 1991 to June 1997 and pressures from 30 to 40 mbar.

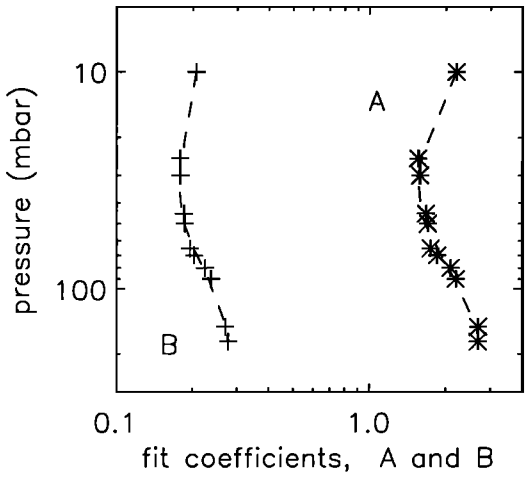

Figure 5. Coefficients A and B for converting extinction at 2.45 μm wavelength to effective radius (equation (5)), determined as a function of pressure from values calculated using the Laramie size distributions (symbols) and a fit in pressure to the coefficients (dashed lines). The pressure dependence of A and B is described according to: $A = -13.325 + 49.0635\,P - 54.3439\,P^2 + 24.748\,P^3 - 3.9459\,P^4$ and $B = -2.2827 + 7.0593\,P - 7.2096\,P^2 + 3.1232\,P^3 - 0.4839\,P^4$, for P in $\log_{10}$(mbar), and pressures from 200 to 10 mbar.

therefore somewhat curious that R_e and $\beta_e(2.45)$ are so well correlated. This correlation exists primarily because of the strong S–β_e and V–β_e correlations, which persist through the ratio $R_e = 3V/S$. The effective radii inferred by using (4) are validated below. Effective radii determined from the 2.45 μm extinctions have uncertainties of the order of 5% less than those determined from the longer-wavelength extinctions. While this is a small effect, the retrievals (described below) are very sensitive to the effective radius and we seek the best inputs possible.

Accepting the uncertainties in inferring R_e, we exploit the advantages of using at least one extinction measurement to determine R_e. Combining R_1 and R_2 with R_e results in highly determined solutions over a broad range of particle size regimes. An example is shown in Figure 6, where R_1, R_2, and R_e were calculated for the size distribution $\sigma = 1.8$ and $\bar{r} = 0.08$ μm, and the curves represent all distributions that reproduced R_1, R_2, and R_e. The benefits of this approach are obvious in comparing results where extinction ratios alone were used (e.g., Figure 3). Also shown are differences between the median radii for the distributions that reproduced R_1 and R_e and the differences between the target value of R_1 and the values of R_1 computed from the distributions that describes R_e. A unique combination of σ and $\bar{r}$ now explains the simulated set of measurements, and the solution exists in a very sharply defined minimum, in terms of both the forward and inverse problems (Figure 6b). This increase in the definition of the minimum is typical for a wide range of size regimes. Although this implies that well-defined solutions can be obtained, the effect of measurement errors cannot be neglected. In reality, a change in one measurement will produce a different, adjacent solution that is equally well defined. These effects are quantitatively assessed below.

4. Size Distribution Retrieval

The principles described above were used to devise a method for solving the inverse problem of determining size distributions from the HALOE multiwavelength extinction measurements. For this purpose, R_i (where $i = 1,2,e$) was calculated at one composition for a wide range of $\bar{r}$ and σ, and these values were used to determine $\bar{r}$ versus R_i, at discrete value of σ. This determination was accomplished by interpolating linearly on the logarithmic values of $\bar{r}$ and R_i for each σ and was performed for a wide range of compositions. Thus, for each measured R_i (R_e is not truly measured; however, it is calculated from a measurement and is referred to as a measurement from here on) a value of $\bar{r}$ can be determined for the corresponding composition and some value of σ (i.e. $\bar{r} = f(R_i, \sigma, W_s)$]. These relationships were tabulated for distributions widths from 1.25 to 3.2 at steps of 0.05, and compositions from 60 to 85% H_2SO_4 at 5% steps. Examples of the relationships between R_i and $\bar{r}$ are shown in Figure 7 for 75% sulfuric acid, where each curve represents a different value of σ. It is apparent that while $\bar{r}$ versus R_i is well defined for some size regimes, it becomes nearly single valued in others, therefore placing high demands on the accuracies of R_i. Additionally, for many size regimes the possible values of R_i are confined to a narrow range. However, where $\bar{r}$ versus R_i is poorly defined, there exists a narrow range of possible R_i, and a solution can still be approximated. In defining $\bar{r}$ versus R_i the solutions have been constrained to describe aerosol populations existing within the bounds: $1.25 < \sigma < 3.2$, $60\% < W_s < 85\%$, and $0.01\ \mu m < \bar{r} < 0.5\ \mu m$. These bounds are consistent with the observed range of size distribution [e.g. *Deshler et al.*, 1993] (see Figure 1) and the range of aerosol composition for typical stratospheric conditions [*Steele and Hamill*, 1981].

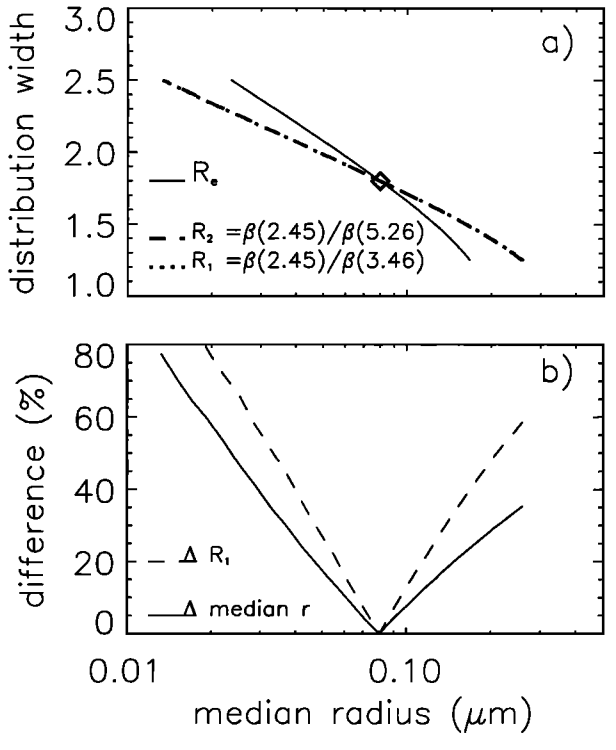

Figure 6. (a) All size distributions that give the same extinction ratios and effective radius as were calculated by using the distribution $\sigma = 1.8$ and $\bar{r} = 0.08$ μm for 75% H_2SO_4. Only the single assumed distribution (diamond) reproduces all three parameters, R_1, R_2, and R_e (i.e., the solution to the inverse problem). (b) Differences between median radii for the distributions that reproduced R_1 and R_e (Δ median r) and the differences between the target value of R_1 and the values of R_1 computed from the distributions that describe R_e, $\Delta R_1 = R_1(r_1, \sigma_1) - R_1(r_e, \sigma_e)$. The differences are shown versus median radius and are directly transposable to the widths in Figure 6a, via the curve for R_1 in Figure 6a.

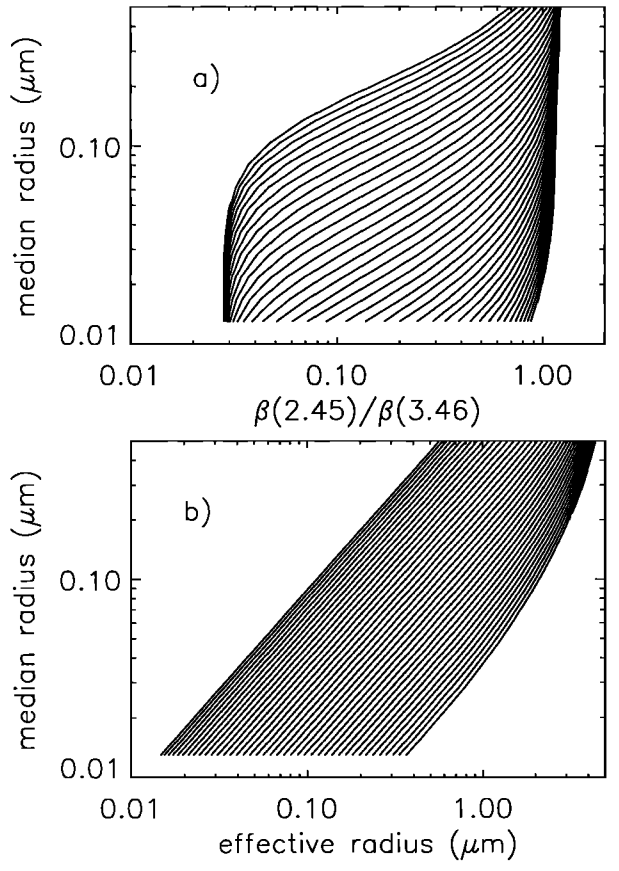

Figure 7. Relationships between the distribution median radius and (a) $R_1 = \beta_e(2.45)/\beta_e(3.46)$ and (b) the effective radius. The values were computed for 75% H_2SO_4, and each curve is for a single value of the distribution width. Widths vary from 1.25 to 3.2 in steps of 0.05, increasing from upper left to lower right. The curves for $R_2 = \beta_e(2.45)/\beta_e(5.26)$ are similar to the curves for R_1.

The inversion procedure calculates three estimates of $\bar{r}$, one from each measurement, for the composition determined from the HALOE water vapor, pressure, and temperature, and an initial value of σ. Since the value of $\bar{r}$ must be unique for one set of observations, the solution is found by varying σ until the three estimates of $\bar{r}$ converge. Using this distribution, we calculate the extinction at one wavelength for a total aerosol concentration (N) of 1 and find the inferred concentration from the ratio of measured to calculated extinctions:

$$N = \frac{\beta_{meas}(\lambda)}{\beta(\lambda, N = 1)} \quad (5)$$

Small improvements in the solution can be gained by using the retrieved distribution to calculate a new estimate of R_e and then performing the inversion again with this new estimate. The Mie calculations are performed only once, to form tables of $\bar{r}$ versus R_t a priori. The inversion uses a table lookup procedure, and the processing time to convergence is a few seconds for a profile containing 50 measurements.

5. Error Analysis

The uncertainties in the retrieved distributions were assessed using two methods. In the first approach the HALOE extinctions were simulated for a 6 year record (1991 to 1997) of size distributions from the Laramie OPC data, and distributions were retrieved from the simulated measurements to determine how well a known solution can be obtained. In the second method the statistical standard deviations in the retrieved distributions were calculated by using a Monte Carlo approach.

5.1. Simulated Retrievals

The Laramie OPC data, as profile measurements, are especially applicable to the problem of simulating the HALOE profile measurements. Although the OPC measurements are usually best described by using bimodal distributions, unimodal distributions can be fitted to the data, and it is useful to test the inversion under the conditions for which it was formulated. Extinctions at the HALOE wavelengths were calculated from 63 profiles of unimodal distributions measured over Laramie, and the size distributions retrieved from these simulated measurements were compared with the original distributions. By using the simulated extinction ratios with the exact values of the effective radii, N, σ, and $\bar{r}$ can be retrieved to within ±5% of the original values. For the HALOE measurements, however, the effective radii must be estimated from the extinctions and not from a known size distribution. In Figure 8 the original distributions are compared to results from inversions performed by using the estimated effective radii (equation (4)). Systematic errors in the estimated effective radii are less than 5%, with random errors (standard deviation of the difference) of less than 10%. These small changes in the effective radius propagate to determine random errors of 40% in the median radii, random errors greater than 40% in the concentrations, and large systematic errors in the concentrations and median radii for pressures greater than 50 mb. The concentration and median radius errors tend to cancel each other in the integrated quantities, as the inferred surface areas and volumes match the original values to within 10% (Figure 8). Indeed, some of the accuracy gained by using the effective radius is lost as a result of errors in the determination of R_e from extinction. These results suggest that the inversions are highly sensitive to the effective radius, since small changes produce large errors in the inferred concentrations and median radii.

Additional inversions were performed by using simulated extinctions based on the bimodal lognormal fits to the Laramie OPC data. Although the inferred and original distributions cannot be directly compared, it is useful to compare the inferred and original concentrations and the distribution moments to determine whether random or systematic effects are introduced by forcing a unimodal distribution. Comparisons of the original and inferred concentrations, surface areas, and volumes for the Laramie profiles show less than 5% bias, with random differences in surface area and volume of less than 10%. The random concentration differences however, are 40% at pressures near 10 mbar and increase to 100% for pressures greater than 60 mbar. These differences are balanced by changes in the distribution width and median radius and are therefore suppressed in the integrated quantities. The unimodal distributions inferred from measurement simulations based on the bimodal distributions were also compared with the unimodal fits to the OPC data. These comparisons show that although no systematic differences are introduced, the random differences in N, σ, and $\bar{r}$ are over 60%, 15%, and 40%, respectively. Simulated retrievals based on the *Goodman et al.* [1994] and *Pueschel et al.* [1994] (typically bimodal) distributions are consistent with results based on the OPC data described above.

5.2. Monte Carlo Analysis

For this analysis, each extinction measurement was randomly perturbed about a normal distribution of width equal to the estimated

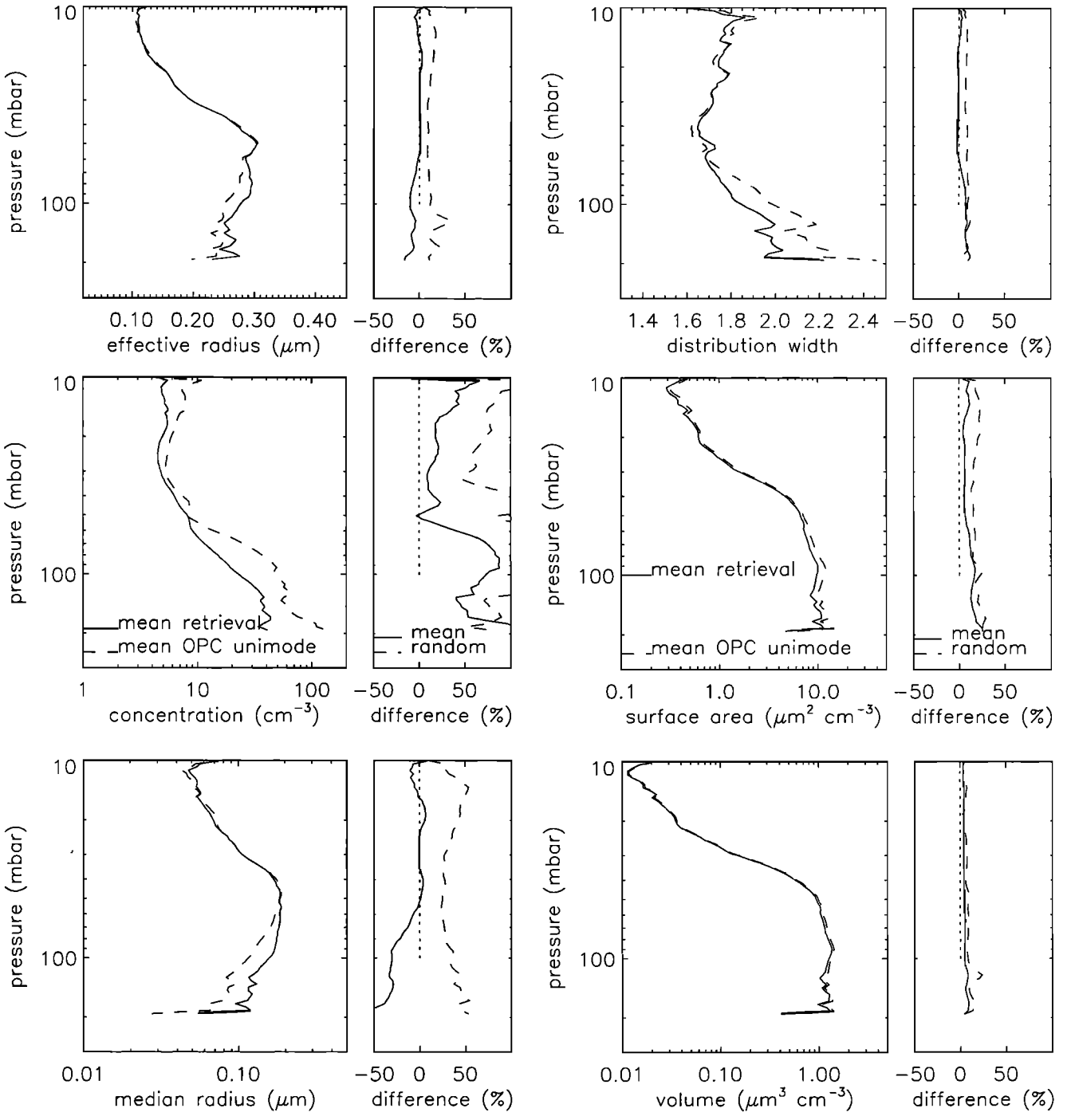

Figure 8. Comparison of the original OPC unimodal size distributions with the distributions retrieved from extinctions calculated from the original distributions. The effective radii were determined from the calculated 2.45 μm extinctions (equation (4)). Statistics for the 63 profile comparisons are shown as mean profiles, mean differences, and random differences (standard deviation of the difference).

error in the measurement. The retrieval is performed on each measurement a number of times, each retrieval receiving application of different random errors. The uncertainties in the inferred distribution parameters are computed as the standard deviation of the mean of the distribution set obtained from the Monte Carlo analysis. The mean solution and solution standard deviation become asymptotic after about 75 error–applied retrievals. Uncertainties in the HALOE extinctions were estimated to be of the order of ±10% [*Hervig et al.*, 1996]. The slope in equation (4) (the exponent, B) is well determined, and the uncertainty in the conversion from 2.45 μm extinction to R_e is carried by the multiplier ($\delta A/A \cong \pm 10\%$). Uncertainties in the HALOE 2.45 μm extinctions, $\delta\beta_e(2.45)/\beta_e(2.45)$, therefore propagate to determine a total uncertainty in the estimate of R_e given by

$$\frac{\delta R_e}{R_e} = B\,\frac{\delta\beta_e(2.45)}{\beta_e(2.45)} + \frac{\delta A}{A} \qquad (6)$$

or about 12% for B=0.2.

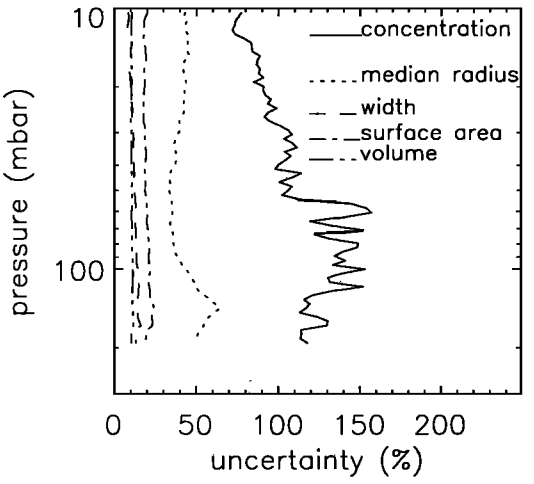

Figure 9. Average uncertainties in the retrieved distributions and distribution moments determined from the Monte Carlo analysis of 24 HALOE profiles measured at 41°N during 1991 to 1995. Uncertainties are presented for the concentration, median radius, distribution width, surface area, and volume, as labeled.

To determine the uncertainties in the inferred size distributions and distribution moments, the Monte Carlo technique was applied to inversions of simulated HALOE extinctions (as described above) and to actual HALOE measurements. The results from the simulated and actual measurements were consistent. Results from inversions of 24 profiles of actual HALOE measurements are presented in Figure 9 as average uncertainty profiles. The inferred concentration and median radius have uncertainties over 90% and 30%, respectively. These values are consistent with the simulated retrieval results presented above, where the concentration and median radius exhibit the greatest sensitivity to measurement errors. Uncertainties in the distribution width, surface area, and volume are less than 25% over the profile extent.

6. Results Using HALOE Measurements

The explicit inversions described above were applied to the HALOE multiwavelength extinction measurements. The HALOE measurements at 2.45, 3.40, and 5.26 μm were used to form the extinction ratios, the effective radius was determined from the 2.45 μm extinctions (equation (4)), and the concentration was determined from the 3.46 μm extinctions (equation (5)). The thermodynamic aerosol composition was determined from the HALOE water vapor and the pressure and temperature for each measurement.

The HALOE size distributions and distribution moments were compared with the Laramie OPC data for coincidences found using maximum allowable separations of 48 hours, 2° latitude, and 25° longitude. Within these bounds, 17 coincidences were found, with average HALOE–OPC separations of 20.1 hours, 0.7° latitude, and 7.1° longitude. An individual comparison from October 1994 is shown in Figure 10 for the OPC unimodal distributions. The effects of determining $\bar{r}$ versus R_i at discrete intervals of σ and W_s are evident in the HALOE retrievals, as the results often vary discretely. While small differences exist, both HALOE and the OPC show the same pressure dependence of the size distribution shape. Figure 11 summarizes 17 comparisons of the HALOE distribution parameters and distribution moments to the unimodal fits to the OPC data. In general, the HALOE distribution parameters are unbiased with respect to the OPCs. While the Monte Carlo analysis suggests that the HALOE concentration uncertainties are over 100%, the HALOE–OPC concentration comparisons have random differences of less than 60%, suggesting greater reliability in the HALOE results.

The integrated quantities calculated from the OPC bimodal distributions should be more representative of the actual measurements than the values obtained from the unimodal distributions [*Deshler et al.*, 1993]. Figure 12 compares the HALOE concentrations, effective radii, surface areas, and volumes with the values calculated from the OPC bimodal fits. The surface areas and volumes determined from the OPC bimodal distributions are 20% to

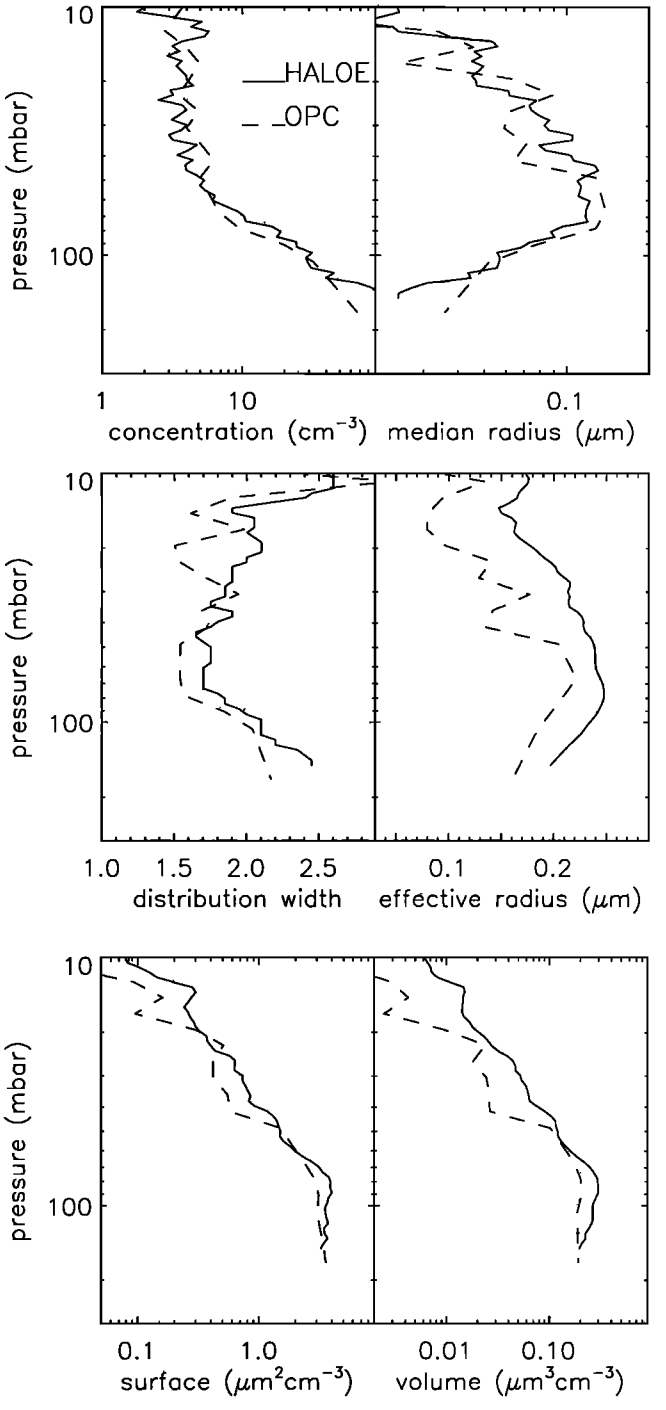

Figure 10. Comparison of the size distributions and distribution moments for coincident HALOE and OPC profiles over Laramie on October 12, 1994. The HALOE values are compared with the OPC unimodal distributions.

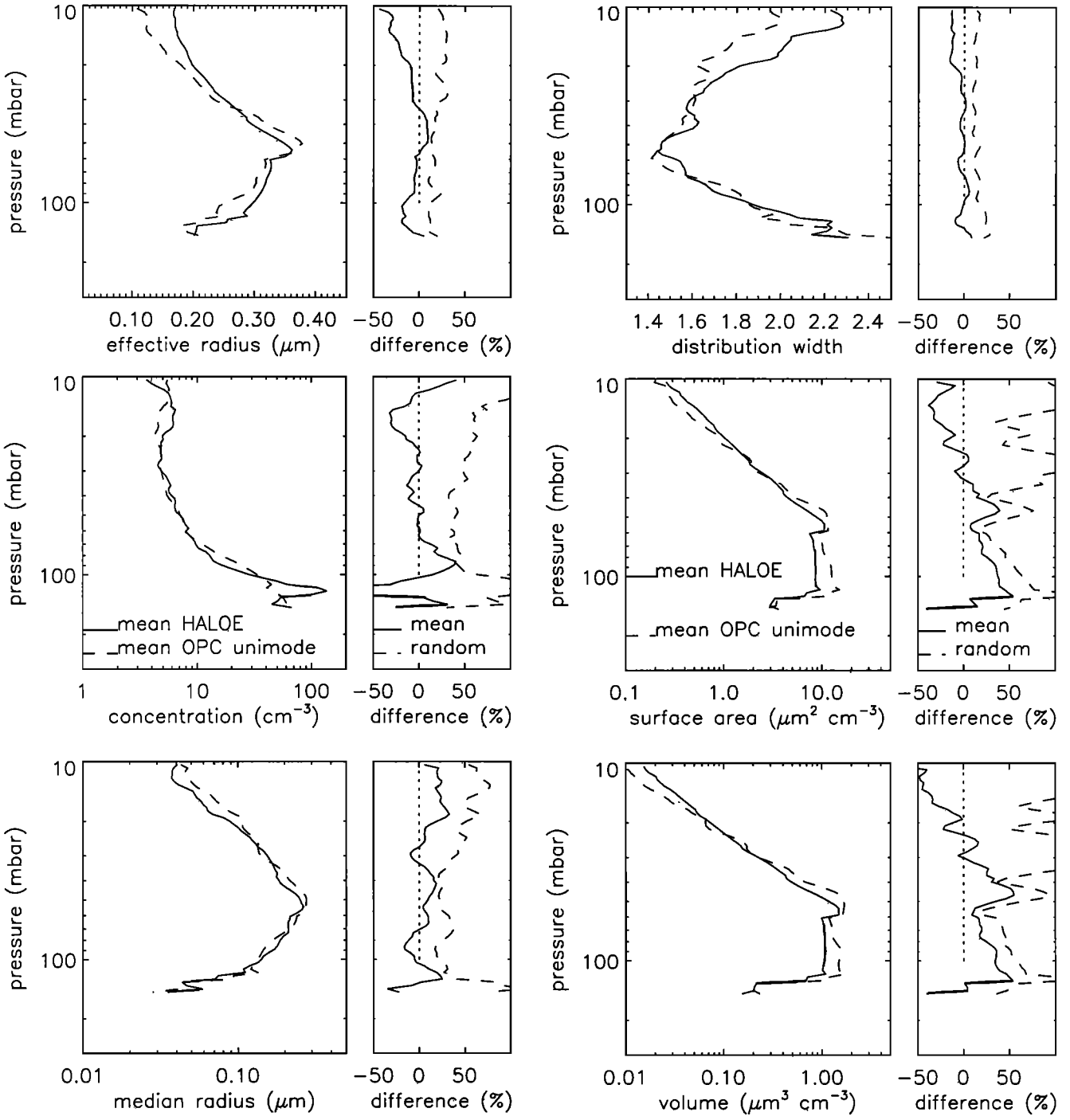

Figure 11. Statistics for 17 coincident HALOE and OPC profile comparisons over Laramie from November 1991 to February 1995 for the OPC unimodal distributions. The comparisons of effective radius, concentration, median radius, width, surface area, and volume are shown as mean profiles, mean differences, and random differences (standard deviation of the difference).

50% less than those determined by using the unimodal fits. The HALOE surface areas and volumes are systematically 20% to 30% greater than the OPC bimodal data, placing HALOE between the OPC unimodal and bimodal results. The volume differences in Figure 12 are consistent with the extinction comparisons reported by *Hervig et al.* [1996], who compared HALOE with results from the OPC bimodal distributions.

7. Conclusions

Aerosol extinction at the HALOE wavelengths alone cannot be used to reliably infer the size distribution except within certain particle size regimes. Such solutions place high demands on the measurement accuracies except for aerosol populations containing sizes larger than about 0.5 μm. The inverse problem becomes highly

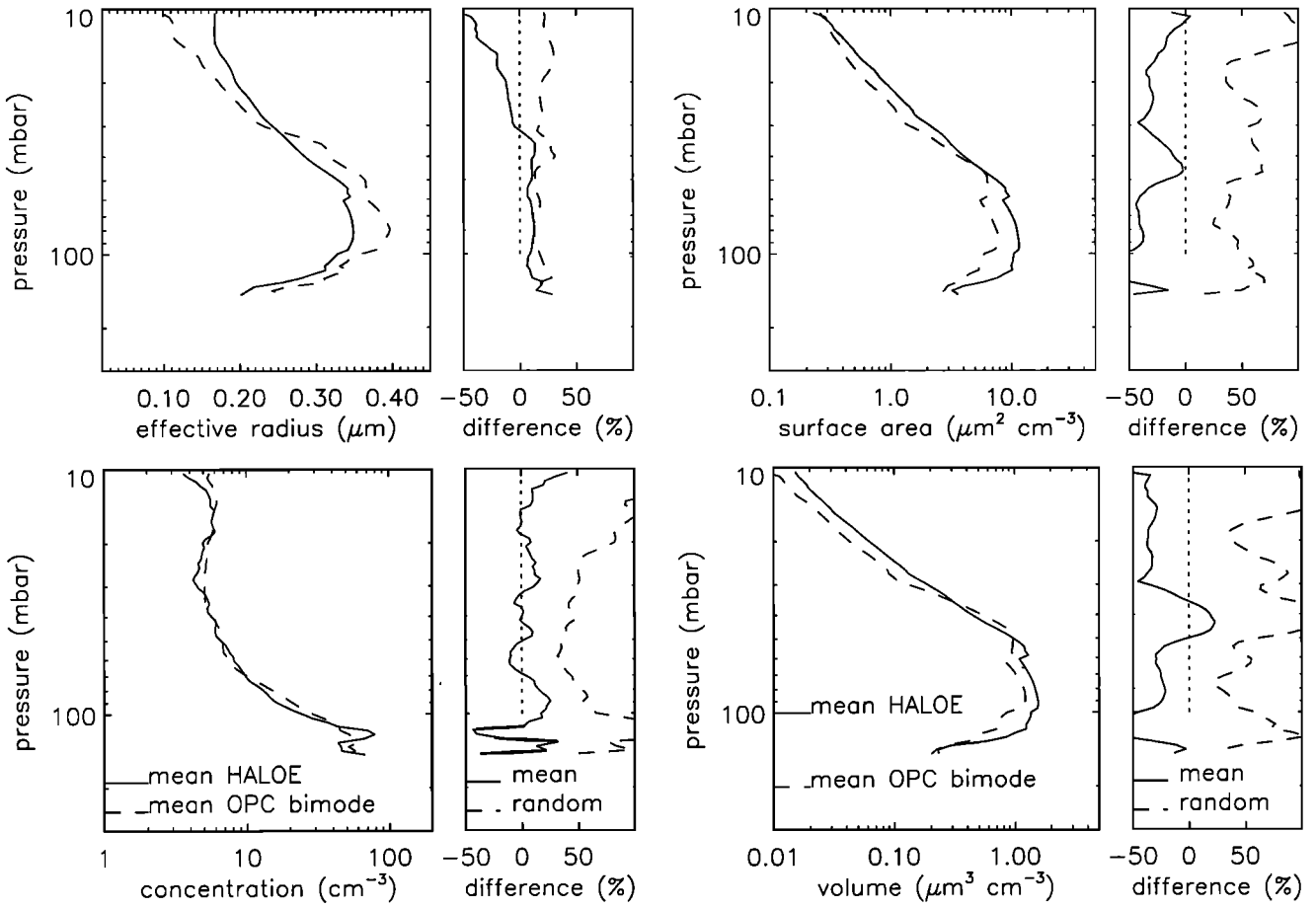

Figure 12. As in Figure 11, except the HALOE values are compared with the OPC bimodal distributions, and comparisons are made for the effective radius, concentration, surface area, and volume.

defined, however, when the effective radius can be used as an inverted measurement. The effective radius can be determined from extinction with uncertainties of about ±10%, and this approach was taken to form solutions to the inverse problem. Using HALOE 2.45 μm extinctions to determine effective radii and forming extinction ratios from the HALOE 2.45, 3.40, and 5.26 μm measurements result in size distributions that are in good agreement with in situ OPC measurements.

In situ measurements suggest that aerosol size distributions become increasingly bimodal in the lower stratosphere and during postvolcanic periods. Although real extinction measurements can be explained in terms of a simple unimodal distribution, these solutions are therefore only an approximation. The error analysis and HALOE–OPC comparisons suggest that although the HALOE distributions do not contain significant biases, the random uncertainties can be large. Using the retrieved unimodal distributions in terms of spatial or temporal averages can reduce the effects of random uncertainties in the results. The size distribution moments appear to be less sensitive to the actual shape of the size distribution. The inferred surface areas and volumes therefore demonstrate smaller random uncertainties than do the actual distributions.

Although aerosol size distributions can be inferred from the HALOE aerosol measurements, these retrievals were possible only because the aerosol effective radius could be reliably inferred a priori. Future experiments measuring aerosols would benefit from deliberate selection of measurement wavelengths that maximize the information concerning the size distribution. Specifically, since aerosol extinctions at infrared wavelengths are characterized by a high degree of linear dependence, it would be beneficial to include both visible (or near–infrared) and infrared wavelengths in one experiment.

The size distribution retrievals described here were formulated for sulfate aerosols alone. Since the physical properties of polar stratospheric clouds (PSCs) are important for studies of polar chemistry, there would be immediate applications for size distributions retrieved from measurements in PSCs. In principle, it should be possible to reformulate the distribution retrievals described here to consider PSCs. This will be the topic of future investigations.

The method described in this paper was used to retrieve size distribution profiles from the HALOE data set, which covers the period from October 1991 to the present. For these retrievals, measurements consistent with tropospheric clouds or PSCs were excluded. Ice was identified by calculating the equilibrium water vapor pressure over ice using the measured water vapor, pressure and temperature. PSCs were identified simply as all observations below 197 K. These data are available to the public at no cost from the HALOE web site, http://haloedata.larc.nasa.gov/Haloe/home.html, under "analyzed aerosol products."

Acknowledgements. This work was supported through funding from the NASA Langley Research Center and the National Science Foundation.

References

Twomey, S., Information content in remote sensing, *Appl. Opt.*, *13*, 942–945, 1974.

Angstrom, A., On the atmospheric transmission of sun radiation and on dust in the air, *Geogr. Ann., 11*, 156–166, 1908.

Curcio, J. A. Evaluation of atmospheric aerosol particle size distribution from scattering measurements in the visible and infrared. *J. Opt. Soc. Am., 51*, 548–551, 1961.

Deshler, T., B. J. Johnson, and W. R. Rozier, Balloonborne measurements of Pinatubo aerosol during 1991 and 1992 at 41°N: Vertical profiles, size distributions, and volatility, *Geophys. Res. Lett., 20*, 1435–1438, 1993.

Goodman, J., K. G. Snetsinger, R. F. Pueschel, G. V. Ferry, and S. Verma, Evolution of Pinatubo aerosol near 19 km altitude over western North America, *Geophys. Res. Lett., 21*, 1129–1132, 1994.

Grainger, R. G., A. Lambert, C. D. Rodgers, F. W. Taylor, and T. Deshler, Stratospheric aerosol effective radius, surface area, and volume estimated from infrared measurements, *J. Geophys. Res., 100*, 16,507–16518, 1995.

Granqvist, C. G., and R. A. Buhrman, Log–normal size distributions of ultrafine metal particles, *Solid State Commun., 18*, 123–126, 1976.

Hanson, D. R., A. R. Ravishankara, and S. Solomon, Heterogeneous reactions in sulfuric acid aerosols: A framework for model calculations. *J. Geophys. Res., 99*, 3615–3629, 1994.

Harries, J. E., J. M. Russell III, A. F. Tuck, L. L. Gordley, P. Purcell, K. Stone, R. M. Bevilacqua, M. Gunson, G. Nedoluha, and W. Traub, Validation of measurements of water vapour from the Halogen Occultation Experiment (HALOE), *J. Geophys. Res., 101*, 10,205–10,216, 1996.

Hervig, M. E., J. M. Russell III, L. L. Gordley, J. Daniels, S. R. Drayson, and J. H. Park, Aerosol effects and corrections in the Halogen Occultation Experiment, *J. Geophys. Res., 100*, 1067–1079, 1995.

Hervig, M. E., J. M. Russell III, L. L. Gordley, J. H. Park, S. R. Drayson, and T. Deshler, Validation of aerosol measurements from the Halogen Occultation Experiment, *J. Geophys. Res., 101*, 10,267–10,275, 1996.

Hofmann, D. J., and T. Deshler, Stratospheric cloud observations during the formation of the Antarctic ozone hole in 1989, *J. Geophys. Res., 96*, 2897–2912, 1991.

Hofmann, D. J., and J. M. Rosen, Sulfuric acid droplet formation and growth in the stratosphere after the 1982 eruption of El Chichon, *Science, 222*, 325–327, 1983.

Hofmann, D. J., and S. Solomon, Ozone destruction through heterogeneous chemistry following the eruption of El Chichón, *J. Geophys. Res., 94*, 5029–5041, 1989.

Junge, C. E., Gesetzmassigkeiten in der Grossenverteilung des atmospharischen Aerosol uber dem Kontinent, *Ber. Dtsch. Wetterdienstes*, U.S. Zone, *35*, 261–277, 1952.

King, M. D., D. M. Byrne, B. M. Herman, and J. A. Reagan, Aerosol size distributions obtained by inversion of spectral optical depth measurements, *J. Appl. Meteorol., 35*, 2153–2167, 1978.

Livingston, J. M., and P. B. Russell, Retrieval of size distribution moments from multiwavelength particulate extinction measurements, *J. Geophys. Res., 94*, 8425–8433, 1989.

Luo, B. P., U. K. Krieger, and Th. Peter, Densities and refractive indices of H_2SO_4 /HNO_3 /H_2O solutions to stratospheric temperatures, *Geophys. Res. Lett., 23*, 3707–3710, 1997.

Palmer, K. F., and D. Williams, Optical constants of sulfuric acid: Application to the clouds of Venus?, *Appl. Opt., 14*, 208–219, 1975.

Pinnick, R. G., J. M. Rosen, and D. J. Hofmann, Stratospheric aerosol measurements III, Optical model calculations, *J. Atmos. Sci., 33*, 304–314, 1976.

Pruppacher, H. R. and J. D. Klett, Microphysics of Clouds and Precipitation, D. Reidel, Norwell, Mass., 1980.

Pueschel, R. F., P. B. Russell, D. A. Allen, G. V. Ferry, K. G. Snetsinger, J. M. Livingston, and S. Verma, Physical and optical properties of the Pinatubo volcanic aerosol: Aircraft observations with impactors and a Sun–tracking photometer, *J. Geophys. Res., 99*, 12,915–12,922, 1994.

Remsberg, E. E., D. Lavery, and B. Crawford Jr., Optical constants for sulfuric and nitric acid, *J. Chem. Eng. Data, 19*, 263–265, 1974.

Rosen, J. M., The boiling point of stratospheric aerosols, *J. Appl. Meteorol., 10*, 1044–1045, 1971.

Russell, P. B., et al., Global to microscale evolution of the Pinatubo volcanic aerosol derived from diverse measurements and analyses, *J. Geophys. Res., 101*, 18,745–18,763, 1996.

Russell, J. M., III, L. L. Gordley, J. H. Park, S. R. Drayson, W. D. Hesketh, R. J. Cicerone, A. F. Tuck, J. E. Frederick, J. E. Harries, and P. J. Crutzen, The Halogen Occultation Experiment, *J. Geophys. Res., 98*, 10,777–10,797, 1993.

Steele, H. M. and P. Hamill, Effects of temperature and humidity on the growth and optical properties of sulfuric acid–water droplets in the stratosphere, *J. Aerosol Sci., 12*, 517–528, 1981.

Twomey, S., Information content in remote sensing, *Appl. Opt., 13*, 942–945, 1974.

Valero, F., and P. Pilewskie, Latitudinal survey of spectral optical depths of the Pinatubo volcanic cloud–derived particle sizes, columnar mass loadings, and effects on planetary albedo, *Geophys. Res. Lett., 19*, 163–166, 1992.

Yue, G. K., M. P. McCormick, and W. P. Chu, Retrieval of composition and size distribution of stratospheric aerosols with the SAGE II satellite experiment, *J. Atmos. Oceanic Technol., 3*, 372–380, 1986.

T. Deshler and M. E. Hervig (corresponding author) Department of Atmospheric Science, University of Wyoming, P.O. Box 3038, Laramie, WY 82071. (e–mail: hervig@trex.uwyo.edu)

James M. Russell III, Center for Atmospheric Sciences, Physics Department, Hampton University, Hampton, VA 23668.

(Received April 22, 1997; revised October 9, 1997;
accepted October 20, 1997.)